A New HIE-PSTD Method for Solving Problems with Fine and Electrically Large Structures Simultaneously

Jianying Guo, Juan Chen, Jianguo Wang, and Anxue Zhang

School of Electronic and Information Engineering
Xi'an Jiaotong University, Xi'an, 710049, People's Republic of China
gjyhn@126.com, chen.juan.0201@mail.xjtu.ed.cn, wanguiuc@163.com, anxuezhang@mail.xjtu.edu.cn

Abstract ─ A new hybrid implicit-explicit difference and pseudospectral (PS) scheme is presented for solving the electromagnetic problems which have fine features and are electrically large. The maximum time-step size in this method is only determined by two spatial discretization which only need two cells per wavelength. The formulation of the method is presented and the time stability condition of the method is demonstrated. This method is more efficient than the finite-difference time-domain (FDTD) method in terms of computer memory and computation time, which is demonstrated through numerical examples.

Index Terms ─ Courant limit, FDTD method, Fourier transform, hybrid implicit explicit difference.

I. INTRODUCTION

The finite-difference time-domain (FDTD) method [1]-[3] has been proven to be a simple algorithm that provides accurate predictions of electromagnetic field interaction. But in practice, the stability condition makes the FDTD method inefficient for some problems with fine or electrically large structures. So there are two prominent efforts that have been made recently to develop more efficient FDTD schemes. First, is to weaken the Courant limit on the time step size of the FDTD method. Second, is to overcome the limit of the wavelength on the space discretization. Among those proposed methods, the hybrid implicit-explicit difference FDTD (HIE-FDTD) method [4]-[6] and pseudospectral time-domain (PSTD) technique [7]-[8] are two kinds of representative algorithms. In the HIE-FDTD method, the time step size is not limited by the fine space discretization and is extremely useful for the analysis of structures with fine-scale dimensions. The PSTD technique uses a Fourier transform algorithm to represent spatial derivative and allows a coarse discretization of only two cells per wavelength[9]-[10], while the FDTD method requires a relatively large number of nodes (usually 10–20 nodes per minimum wavelength for a problem of moderate size) to achieve reasonably good accuracy. This makes the PSTD method more efficient than the FDTD method

for problems with electrically large structures. However, many simulations of electromagnetic problems are both with fine and electrically large structures, such as the fine plane. So it is desirable to combine the HIE-FDTD and PSTD algorithms to efficiently handle this structure.

In this paper, we present a novel HIE-PSTD method which applies the hybrid implicit explicit difference technique in one direction and the pseudospectral scheme in the other two directions. The new method not only weakens the Courant limit on the time step size, but also overcomes the limit of the wavelength on the space discretization. The time step size in this method is not determined by the fine space discretization and the space discretization along the electrically large direction only need two cells per wavelength. First, the 3-D formula of the HIE-PSTD method is presented and the time stability condition of the method is discussed. Finally, the numerical performance of the method is demonstrated through numerical examples by comparing with the FDTD and HIE-FDTD methods.

II. FORMULAS

In a linear, non-dispersive, and lossless medium, the Maxwell's curl equations for full waves are as follows:

$$\varepsilon \frac{\partial E_x}{\partial t} = \frac{\partial H_z}{\partial y} - \frac{\partial H_y}{\partial z}, \tag{1.1}$$

$$\varepsilon \frac{\partial E_y}{\partial t} = \frac{\partial H_x}{\partial z} - \frac{\partial H_z}{\partial x}, \tag{1.2}$$

$$\varepsilon \frac{\partial E_z}{\partial t} = \frac{\partial H_y}{\partial x} - \frac{\partial H_x}{\partial y}, \tag{1.3}$$

$$\mu \frac{\partial H_x}{\partial t} = \frac{\partial E_y}{\partial z} - \frac{\partial E_z}{\partial y}, \tag{1.4}$$

$$\mu \frac{\partial H_y}{\partial t} = \frac{\partial E_z}{\partial x} - \frac{\partial E_x}{\partial z}, \tag{1.5}$$

$$\mu \frac{\partial H_z}{\partial t} = \frac{\partial E_x}{\partial y} - \frac{\partial E_y}{\partial x}. \tag{1.6}$$

Assuming that the fine structure is along the *z* direction and the electrically large structures are along

the x direction and the y direction. So the high-density cells in the z direction have to be used in order to accurately describe this fine structure. In order to make sure that the time step size have no relation with spatial increment Δz, apply the hybrid implicit explicit difference technique to the derivative in z direction. Meanwhile in the x direction and the y direction, the PSTD method is employed. We use the forward and inverse Fourier transforms to replace the derivative with respect to x and y. Being different from the standard Yee's algorithm, the HIE-PSTD method does not require the spatial staggered grid along the x direction and the y direction. The electromagnetic field components are arranged on the cells as shown in Fig. 1.
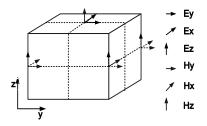

Fig. 1. Spatial grid of the field components in the HIE-PSTD method.

Thus, the difference updating Equations of (1) can be obtained as:

$$\varepsilon \frac{E_x^{n+1}\left(i+\frac{1}{2},j+\frac{1}{2},k\right)-E_x^n\left(i+\frac{1}{2},j+\frac{1}{2},k\right)}{\Delta t}=$$

$$\mathfrak{I}_y^{-1}\left\{\mathfrak{I}_y\left[\partial H_z^{n+1}\left(i+\frac{1}{2},j+\frac{1}{2},k\right)\Big/\partial y\right]\right\}$$

$$-\frac{1}{2\Delta z}\left[\begin{array}{l}H_y^{n+1}\left(i,j,k+\frac{1}{2}\right)-H_y^{n+1}\left(i,j,k-\frac{1}{2}\right)\\+H_y^n\left(i,j,k+\frac{1}{2}\right)-H_y^n\left(i,j,k-\frac{1}{2}\right)\end{array}\right], \quad (2.1)$$

$$\varepsilon \frac{E_y^{n+1}\left(i+\frac{1}{2},j+\frac{1}{2},k\right)-E_y^n\left(i+\frac{1}{2},j+\frac{1}{2},k\right)}{\Delta t}=$$

$$\frac{1}{2\Delta z}\left[\begin{array}{l}H_x^{n+1}\left(i,j,k+\frac{1}{2}\right)-H_x^{n+1}\left(i,j,k-\frac{1}{2}\right)\\+H_x^n\left(i,j,k+\frac{1}{2}\right)-H_x^n\left(i,j,k-\frac{1}{2}\right)\end{array}\right]$$

$$-\mathfrak{I}_x^{-1}\left\{\mathfrak{I}_x\left[\partial H_z^{n+1}\left(i+\frac{1}{2},j+\frac{1}{2},k\right)\Big/\partial x\right]\right\}, \quad (2.2)$$

$$\varepsilon \frac{E_z^{n+1}\left(i,j,k+\frac{1}{2}\right)-E_z^n\left(i,j,k+\frac{1}{2}\right)}{\Delta t}$$

$$=\mathfrak{I}_x^{-1}\left\{\mathfrak{I}_x\left[\partial H_y^n\left(i,j,k+\frac{1}{2}\right)\Big/\partial x\right]\right\}$$

$$-\mathfrak{I}_y^{-1}\left\{\mathfrak{I}_y\left[\partial H_x^n\left(i,j,k+\frac{1}{2}\right)\Big/\partial y\right]\right\}, \quad (2.3)$$

$$\mu \frac{H_x^{n+1}\left(i,j,k+\frac{1}{2}\right)-H_x^n\left(i,j,k+\frac{1}{2}\right)}{\Delta t}$$

$$=\frac{1}{2\Delta z}\left[\begin{array}{l}E_y^{n+1}\left(i+\frac{1}{2},j+\frac{1}{2},k+1\right)-E_y^{n+1}\left(i+\frac{1}{2},j+\frac{1}{2},k\right)\\+E_y^n\left(i+\frac{1}{2},j+\frac{1}{2},k+1\right)-E_y^n\left(i+\frac{1}{2},j+\frac{1}{2},k\right)\end{array}\right]$$

$$-\mathfrak{I}_y^{-1}\left\{\mathfrak{I}_y\left[\partial E_z^{n+1}\left(i,j,k+\frac{1}{2}\right)\Big/\partial y\right]\right\}, \quad (2.4)$$

$$\mu \frac{H_y^{n+1}\left(i,j,k+\frac{1}{2}\right)-H_y^n\left(i,j,k+\frac{1}{2}\right)}{\Delta t}=$$

$$\mathfrak{I}_x^{-1}\left\{\mathfrak{I}_x\left[\partial E_z^{n+1}\left(i,j,k+\frac{1}{2}\right)\Big/\partial x\right]\right\}$$

$$-\frac{1}{2\Delta z}\left[\begin{array}{l}E_x^{n+1}\left(i+\frac{1}{2},j+\frac{1}{2},k+1\right)-E_x^{n+1}\left(i+\frac{1}{2},j+\frac{1}{2},k\right)\\+E_x^n\left(i+\frac{1}{2},j+\frac{1}{2},k+1\right)-E_x^n\left(i+\frac{1}{2},j+\frac{1}{2},k\right)\end{array}\right], \quad (2.5)$$

$$\mu \frac{H_z^{n+1}\left(i+\frac{1}{2},j+\frac{1}{2},k\right)-H_z^n\left(i+\frac{1}{2},j+\frac{1}{2},k\right)}{\Delta t}=$$

$$\mathfrak{I}_y^{-1}\left\{\mathfrak{I}_y\left[\partial E_x^n\left(i+\frac{1}{2},j+\frac{1}{2},k\right)\Big/\partial y\right]\right\}$$

$$-\mathfrak{I}_x^{-1}\left\{\mathfrak{I}_x\left[\partial E_y^n\left(i+\frac{1}{2},j+\frac{1}{2},k\right)\Big/\partial x\right]\right\}. \quad (2.6)$$

Obviously, the updating of E_x and E_y, as shown in the Equations (2.1) and (2.2), needs the unknown H_x and H_y at the same time; thus, E_x and E_y have to be updated implicitly. By substituting the Equation (2.5) into (2.1) and the Equation (2.5) into (2.2), the equations for E_x and E_y are given as:

$$\left[1+\frac{\Delta t^2}{2\varepsilon\mu\Delta z^2}\right]E_x^{n+1}\left(i+\frac{1}{2},j+\frac{1}{2},k\right)-\frac{\Delta t^2}{4\varepsilon\mu\Delta z^2}\left[\begin{array}{c}E_x^{n+1}\left(i+\frac{1}{2},j+\frac{1}{2},k+1\right)\\+E_x^{n+1}\left(i+\frac{1}{2},j+\frac{1}{2},k-1\right)\end{array}\right]$$

$$=E_x^n\left(i+\frac{1}{2},j+\frac{1}{2},k\right)+\frac{\Delta t}{\varepsilon}\Im_y^{-1}\left\{\Im_y\left[\partial H_z^{n+1}\left(i+\frac{1}{2},j+\frac{1}{2},k\right)\Big/\partial y\right]\right\}$$

$$+\frac{\Delta t^2}{4\varepsilon\mu\Delta z^2}\left[\begin{array}{c}E_x^n\left(i+\frac{1}{2},j+\frac{1}{2},k+1\right)-E_x^n\left(i+\frac{1}{2},j+\frac{1}{2},k\right)\\-E_x^n\left(i+\frac{1}{2},j+\frac{1}{2},k\right)+E_x^n\left(i+\frac{1}{2},j+\frac{1}{2},k-1\right)\end{array}\right]$$

$$-\frac{\Delta t}{\varepsilon\Delta z}\left[H_y^n\left(i,j,k+\frac{1}{2}\right)-H_y^n\left(i,j,k-\frac{1}{2}\right)\right]$$

$$-\frac{\Delta t^2}{2\varepsilon\mu\Delta z}\left[\begin{array}{c}\Im_x^{-1}\left\{\Im_x\left[\partial E_z^{n+1}\left(i,j,k+\frac{1}{2}\right)\Big/\partial x\right]\right\}\\-\Im_x^{-1}\left\{\Im_x\left[\partial E_z^{n+1}\left(i,j,k-\frac{1}{2}\right)\Big/\partial x\right]\right\}\end{array}\right],$$

(2.7)

$$\left[1+\frac{\Delta t^2}{2\varepsilon\mu\Delta z^2}\right]E_y^{n+1}\left(i+\frac{1}{2},j+\frac{1}{2},k\right)$$

$$-\frac{\Delta t^2}{4\varepsilon\mu\Delta z^2}\left[\begin{array}{c}E_y^{n+1}\left(i+\frac{1}{2},j+\frac{1}{2},k+1\right)\\+E_y^{n+1}\left(i+\frac{1}{2},j+\frac{1}{2},k-1\right)\end{array}\right]$$

$$=E_y^n\left(i+\frac{1}{2},j+\frac{1}{2},k\right)-\frac{\Delta t}{\varepsilon}\Im_x^{-1}\left\{\Im_x\left[\partial H_z^{n+1}\left(i+\frac{1}{2},j+\frac{1}{2},k\right)\Big/\partial x\right]\right\}$$

$$+\frac{\Delta t^2}{4\varepsilon\mu\Delta z^2}\left[\begin{array}{c}E_y^n\left(i+\frac{1}{2},j+\frac{1}{2},k+1\right)-E_y^n\left(i+\frac{1}{2},j+\frac{1}{2},k\right)\\-E_y^n\left(i+\frac{1}{2},j+\frac{1}{2},k\right)+E_y^n\left(i+\frac{1}{2},j+\frac{1}{2},k-1\right)\end{array}\right]$$

$$+\frac{\Delta t}{\varepsilon\Delta z}\left[H_x^n\left(i,j,k+\frac{1}{2}\right)-H_x^n\left(i,j,k-\frac{1}{2}\right)\right]$$

$$-\frac{\Delta t^2}{2\varepsilon\mu\Delta z}\left[\begin{array}{c}\Im_y^{-1}\left\{\Im_y\left[\partial E_z^{n+1}\left(i,j+1,k+\frac{1}{2}\right)\Big/\partial y\right]\right\}\\-\Im_y^{-1}\left\{\Im_y\left[\partial E_z^{n+1}\left(i,j+1,k-\frac{1}{2}\right)\Big/\partial y\right]\right\}\end{array}\right],$$

(2.8)

where $\Im_\alpha$ and $\Im_\alpha^{-1}$ is forward and inverse Fourier transforms to variable α (where α is x or y). Taking spatial derivative $\partial E_x^{n+1}/\partial y$ as an example, the Fourier transforms can be obtained as:

$$\Im_y^{-1}\left\{\Im_y\left[\frac{\partial E_x^{n+1}\left(i+\frac{1}{2},j+\frac{1}{2},k\right)}{\partial y}\right]\right\}$$

$$=A\times B\times\left[\begin{array}{c}E_x^{n+1}\left(I+\frac{1}{2},1+\frac{1}{2},k\right)\\E_x^{n+1}\left(I+\frac{1}{2},2+\frac{1}{2},k\right)\\.\\.\\.\\E_y^{n+1}\left(I+\frac{1}{2},\left(J-1+\frac{1}{2}\right),k\right)\end{array}\right],$$

(3)

where B is a $L\times I$ matrix, and $B_{l,i}=e^{-\hat{j}(k_{y,l})(i\Delta y)}\Delta y$, A is a $1\times L$ vector, and $A_{1,l}=\frac{1}{2\pi}\left(\hat{j}k_{y,l}\right)e^{\hat{j}(k_{y,l})(i\Delta y)}\Delta y$. The range of spectral k_y domain is from $-\frac{2\pi}{2\Delta y}$, to $\frac{2\pi}{2\Delta y}$, $k_{y,l}=-\frac{2\pi}{2\Delta y}+l\Delta k_y$, $\Delta k_y=\frac{2\pi}{L\Delta y}$, $L=I$ is the total mesh cell in the y direction.

Therefore, components E_z and H_z are explicitly updated first by using the Equations (2.3) and (2.6). Then, E_x and E_y components are updated implicitly by solving the tridiagonal matrix Equations (2.7) and (2.8). At last, H_x and H_y are explicitly updated straight forward by using the equations (2.4) and (2.5).

III. NUMERICAL STABILITY

We now study the numerical stability in the proposed HIE-PSTD algorithm. The field components of traveling-wave as shown:

$$E_p(i,j,k)=\zeta^n E_{p0}e^{\hat{j}(k_x i\Delta x+k_y j\Delta y+k_z k\Delta z)},\qquad(4)$$

$$H_p(i,j,k)=\zeta^n H_{p0}e^{\hat{j}(k_x i\Delta x+k_y j\Delta y+k_z k\Delta z)},\qquad(5)$$

where $p=x,y,z$, $\hat{j}=\sqrt{-1}$, E_{p0} and H_{p0} are the amplitudes of the field components respectively. k_x, k_y and k_z are wave numbers, and ζ indicates growth factor. We substitute the Equations (5) and (4) into (2.1)-(2.6), and obtain the equations as:

$$(\zeta-1)H_{x0}=\frac{\Delta t}{\mu}\left(\hat{j}\zeta k_y E_{z0}+(\zeta+1)\cdot\frac{E_{y0}}{\Delta z}\cdot\sin\left(\frac{k_z\Delta z}{2}\right)\right),(6)$$

$$(\zeta-1)H_{y0}=\frac{\Delta t}{\mu}\left(-\hat{j}\zeta k_x E_{z0}-(\zeta+1)\cdot\frac{E_{x0}}{\Delta z}\cdot\sin\left(\frac{k_z\Delta z}{2}\right)\right),(7)$$

$$(\zeta-1)H_{z0}=\frac{\Delta t}{\mu}\left(-\hat{j}\zeta k_y E_{x0}+\hat{j}\zeta k_x E_{y0}\right),\qquad(8)$$

$$(\zeta-1)E_{x0}=\frac{\Delta t}{\varepsilon}\left(-\hat{j}\zeta k_y H_{z0}-(\zeta+1)\frac{H_{y0}}{\Delta z}\sin\left(\frac{k_z\Delta z}{2}\right)\right),(9)$$

$$(\zeta-1)E_{y0}=\frac{\Delta t}{\varepsilon}\left(\hat{j}\zeta k_x H_{z0}+(\zeta+1)\frac{H_{x0}}{\Delta z}\sin\left(\frac{k_z\Delta z}{2}\right)\right),(10)$$

$$(\zeta-1)E_{z0}=\frac{\Delta t}{\varepsilon}\left(\hat{j}k_y H_{x0}-\hat{j}k_x H_{y0}\right).\qquad(11)$$

By substituting the Equations (6)-(8) into (9)-(11), and eliminating H_{x0}, H_{y0} and H_{z0}, we obtain three equations of E_{x0}, E_{y0} and E_{z0}. Then combining the three equations, and eliminating E_{x0}, E_{y0} and E_{z0}, we obtain:

$$(\zeta-1)^2 \times \left[\begin{array}{l} \dfrac{abD^2}{4}(\zeta+1)^2 \\ +\left(ab(\hat{j}k_x)^2 + ab(\hat{j}k_y)^2\right)\zeta - (\zeta-1)^2 \end{array} \right]^2 = 0, \quad (12)$$

where $a = \Delta t/\varepsilon$, $b = \Delta t/\mu$, $D = 2\hat{j}\sin(k_z\Delta z/2)/\Delta z$. By solving the Equation (12), the growth factor ζ can be obtained:

$$\zeta_1 = 1,$$

$$\zeta_{2,3} = \frac{N \pm \sqrt{N^2 - R^2}}{R},$$

where

$$R = abD^2/2 - 2,$$

$$N = -\left(abD^2/2 + ab(\hat{j}k_y)^2 + ab(\hat{j}k_x)^2 + 2\right).$$

To satisfy the stability condition during field advancement, the module of growth factor ζ cannot be larger than 1. Thus, it has

$$R^2 \geq N^2 \Rightarrow \frac{abk_y^2}{4} + \frac{abk_x^2}{4} \leq 1.$$

Due to the maximum value of k_x and k_y is $\dfrac{2\pi}{2\Delta x}$, it obtains:

$$\frac{ab}{4}\left(\frac{\pi}{\Delta y}\right)^2 + \frac{ab}{4}\left(\frac{\pi}{\Delta x}\right)^2 \leq 1 \Rightarrow \Delta t \leq \frac{1}{c\sqrt{(\pi/2\Delta y)^2 + (\pi/2\Delta x)^2}}.$$
$$(13)$$

From the Equation (13), we can see, the maximum time-step size in this method is only determined by spatial increments Δx and Δy. When the simulated structure has fine-scale dimensions in the z direction, this is especially useful. The spatial increments Δx and Δy. only needs to satisfy Nyquist sampling theorem which results the spatial discretization $\Delta x \leq \lambda/2$ and $\Delta y \leq \lambda/2$. Thus, for the electrically large dimensions in the x direction and the y direction, and thin dimensions in the z direction, the HIE-PSTD algorithm is more efficient than the FDTD method. For example, in the z direction, in order to accurately describe the fine structure, the spatial increments $\Delta z = \lambda/100$ for the FDTD method and the HIE-PSTD method. In the x direction and the y direction, for the FDTD method, considering the limit of the wavelength on the space discretization, the spatial discretization Δx and Δy are selected to be 1/10 of the wavelength, while for the HIE-PSTD method, spatial discretization Δx and Δy can be increased to 1/2 of the wavelength. With the space discretization determined beforehand, the maximum time-step size to satisfy the stability condition of the FDTD algorithm is Δt_0 and of the HIE-PSTD method is Δt_1. Then Δt_1 is 22.7 times of

Δt_0. So the computation time requirement of the HIE-PSTD method is considerably reduced.

IV. NUMERICAL VALIDATION

To demonstrate the time stability condition of the HIE-PSTD method, a simple numerical example is presented. A computation domain with total mesh number $90\times90\times50$ is discretized. To cut off the outer boundary, the perfectly matched layer (PML) proposed by Berenger [11] can be used. A small current source applied along the x direction is placed at the cell (20, 20, 20) of the computation domain. The time dependence of the excitation function is:

$$J_x(t) = \sin(2\pi f_0 t), \quad (14)$$

where $f_0 = 100\times10^9\,Hz$, thus the wavelength of the source is $0.003m$. The observation point is at the cell (30, 30, 40). We apply the FDTD and the HIE-PSTD methods to compute the electric field component E_x at the observation point. The spatial cell size is $\Delta x = \Delta y = 10\Delta z = 0.3mm$, corresponding to 1/10 of the wavelength. For FDTD method, the time step size is

$$\Delta t = 1\Big/c\sqrt{(1/0.0003)^2 + (1/0.0003)^2 + (1/0.00003)^2} = 0.099ps,$$

which is the maximum time-step size to satisfy the stability condition of the FDTD algorithm. For the HIE-PSTD method, the time-step sizes are

$$\Delta t = 2\Big/c\sqrt{(\pi/0.0003)^2 + (\pi/0.0003)^2} = 0.45ps.$$ Figure 2 shows the electric field component E_x at observation point calculated by using the conventional FDTD and the HIE-PSTD methods.

It can be seen from the figure that the result calculated by using the HIE-PSTD method agrees very well with the result calculated by using the conventional FDTD method, which shows the HIE-PSTD method has high computational accuracy with a time step that permitted by the time stability condition.
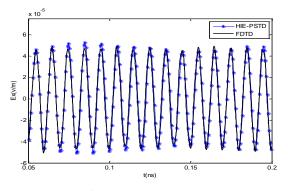

Fig. 2. Electric field component E_x at the observation point calculated by using the FDTD $(\Delta x = \Delta y = 10\Delta z = 0.03mm, \Delta t = 0.099ps)$ and the HIE-PSTD $(\Delta x = \Delta y = 10\Delta z = 0.3mm, \Delta t = 0.45ps)$ methods.

In the HIE-PSTD method, we apply the HIE finite-difference. This technique will bring a splitting error which is proportional to the time-step size [12], and is almost not affected by the increase of the space increment [13]-[15]. Now we study the computational accuracy of the HIE-PSTD method with different time-step size.

For the FDTD method, we set spatial increment $\Delta x = \Delta y = 10\Delta z = 0.3mm$ and the time-step $\Delta t_0 = 0.099\,ps$ which is the maximum time-step maximum to satisfy the stability condition of the FDTD algorithm. For the HID-PSTD method, we set spatial increment $\Delta z = 0.03mm$ unchanged and space increment Δx and Δy to be $0.15mm$ corresponding to $\lambda/2$ which is the maximum space increment. Define $CFLN = \Delta t/\Delta t_0$, where Δt is the time-step of the HIE-PSTD method. When $\Delta t = \Delta t_{max}$, corresponding to the maximum time-step size to ensure the numerical stability in the HIE-PSTD method, $CFLN=22$. We set $CFLN$ to be 8, 12, 20, and 22 (corresponding time-step size increases from $0.79ps$ to $2.25ps$) and calculate the electric field component E_x at observation point by using the HIE-PSTD method with different $CFLN$ respectively.

Figure 3 and Fig. 4 show the result calculated by using the HIE-PSTD method with different $CFLN$. For the comparison, the result calculated by using the FDTD method is shown in Fig. 3-Fig. 4 simultaneously.

It can be seen from Fig. 3 that, when $CFLN$=8, 12, the computational result of the HIE-PSTD method agrees well with the result of the FDTD method.

When $CFLN$ is too large ($CFLN$=20, 22), as shown in the Fig. 4, the accuracy of the HIE-PSTD method began to decrease for the large time-step. Table l shows the simulation time of the FDTD and the HIE-PSTD methods.
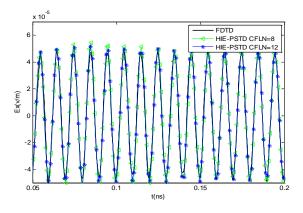

Fig. 3. Electric field component E_x at the observation point calculated by using the FDTD and the HIE-PSTD methods with different time step sizes.
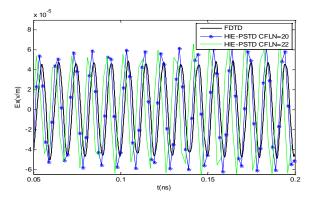

Fig. 4. Electric field component E_x at the observation point calculated by using the FDTD and the HIE-PSTD methods with different time step sizes.

Table 1: Error and computation time of the HIE-PSTD method for difference $CFLN$

Time	CFLN=1	CFLN=8	CFLN=12	CFLN=20	CFLN=22
FDTD	7893s				
HIE-PSTD	8929s	987s	706s	412s	344s

We can see, the HIE-PSTD takes much less time than that of the FDTD method. So in practice, the choice of $CFLN$ (or Δt) in the HIE-PSTD method is dictated by the accuracy and efficiency rather than the stability consideration. In the situation with very stringent accuracy requirements, $CFLN$ should not be larger than 12 usually.

V. SPECIFIC EXAMPLE

Considering the HIE-PSTD method is mainly useful in the simulations of electromagnetic problems which are both with fine structures and electrically large structure, another example with similar geometry is presented to demonstrate the accuracy and efficiency of the HIE-PSTD. We simulate a 3-D parallel-plate structure. The size of the plate is $0.06mm \times 90mm \times 90mm$ (as shown in Fig. 5). The distance between the plates is $12mm$. The z direction incident plane wave is Gauss pulse with the highest frequency of $100 \times 10^9\,Hz$. Thus, the wavelength of the incident plane wave is about $3mm$. The polarization is along the x direction. The observation point is at the center of the gap between two parallel plates.

To demonstrate the numerical performance of the HIE-PSTD method, we perform the numerical simulations for a $0.1ns$ time history by using the FDTD and the HIE-PSTD methods. The plate has fine structure along the z direction, so we set $\Delta z = 0.03mm$. Considering the limit of the wavelength on the space discretization, for the FDTD method, the spatial

discretization $\Delta x = \Delta y = 0.3mm$ and for the HIE-PSTD method spatial discretization Δx and Δy can be increased to $1.5mm$, corresponding to $1/2$ of the wavelength. The time step size for FDTD method is

$$\Delta t = 1 / c\sqrt{\left(1/0.0003\right)^2 + \left(1/0.0003\right)^2 + \left(1/0.00003\right)^2} = 0.099\,ps,$$

For the HIE-PSTD method, the time step size is the maximum time-step size to satisfy the stability condition of the HIE-PSTD algorithm,

$$\Delta t = 2 / c\sqrt{\left(\pi/0.0015\right)^2 + \left(\pi/0.0015\right)^2} = 2.25\,ps, \quad \text{namely,}$$

which is 22 times as that of the FDTD. Figure 6 shows the electric field component at the observation point calculated by using the FDTD, and the HIE-PSTD methods. It can be seen from Fig. 6 that the result of the HIE-PSTD method agrees very well with the result calculated by using the FDTD method.
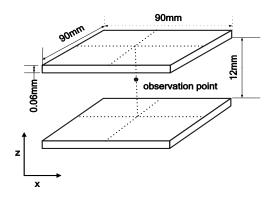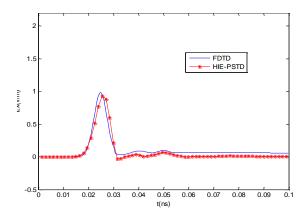

Fig. 5. The parallel-plate structure.

Fig. 6. Electric field component E_x at the observation point calculated by using the FDTD and HIE-PSTD methods.

The computation time and memory requirement of the simulation above are summarized in Table 2. It can be seen from this table that both the memory requirement and computational time for the HIE-PSTD method are reduced significantly compared with those of the FDTD

method, due to large spatial discretization and large time step size applied, the memory requirement of the HIE-PSTD method is reduced by 42%, and the computation time is almost 1/16 of that of the FDTD method.

It should be noted that the standard DFT algorithm is only based on a uniform sampling. So the HIE-PSTD method is limited in application to the cases that require a non-uniform grid. To overcome this difficulty, non-uniform DFT have been suggested [16], these methods may add complexity and instability.

Table 2: Simulation time and memory requirement for the FDTD method and HIE-PSTD method

	Total Cells	Δt (ps)	Time (s)	Memory (Mb)
FDTD	360×360×74	0.099	7626	213.72
HIE-PSTD	130×130×74	2.25	473	90.15

VI. CONCLUSION

This paper introduces a HIE-PSTD method based on the hybrid implicit explicit difference technique and pseudospectral scheme. The maximum time-step size in this method is only determined by spatial discretization Δx and Δy, which only needs two cells per wavelength.

The numerical performance of the method is demonstrated through numerical examples by comparing with the FDTD. For solving these problems both with fine structures and electrically large structure, the HIE-PSTD method will be more efficient than the FDTD methods in terms of computer memory and computation time.

ACKNOWLEDGMENT

REFERENCES

[1] K. S. Yee, "Numerical solution of initial boundary value problems involving Maxwell's equations in isotropic media," *IEEE Trans. Antennas Propagat.*, vol. 14, pp. 302-307, May 1996.

[2] A. Taflove, *Computational Electrodynamics*. Norwood, MA, USA: Artech House, 1995.

[3] K. P. Ma, M. Li, J. L. Drewniak, T. H. Hubing, and T. P. VanDoren, "Comparison of FDTD algorithms for sub cellular modeling of slots in shielding enclosures," *IEEE Trans. Electromagn. Compat.*, vol. 39, no. 5, pp. 147-155, May 1997.

[4] J. Chen and J. Wang, "A 3-D hybrid implicit-explicit FDTD scheme with weakly conditional stability," *Microw. Opt. Tech. Lett.*, vol. 48, pp.

2291-2294, Nov. 2006.

[5] J. Chen and J. Wang, "A three-dimensional semi-implicit FDTD scheme for calculation of shielding effectiveness of enclosure with thin slots," *IEEE Trans. Electromagn. Compat.*, vol. 49, no. 2, pp. 354-360, Feb. 2007.

[6] J. Chen and J.Wang, "Numerical simulation using HIE-FDTD method to estimate various antennas with fine scale structures," *IEEE Trans. Antennas Propagat.*, vol. 55, no. 12, pp. 3603-3612, Dec. 2007.

[7] Q. H. Liu, "Large-scale simulations of electro-magnetic and acoustic measurements using the pseudospectral time-domain (PSTD) algorithm," *IEEE Trans. Geosci. Remote Sensing*, vol. 37, no. 2, pp. 917-926, Mar. 1999.

[8] Z. Lin, "The optimal spatially-smoothed source patterns for the pseudospectral time-domain method," *IEEE Trans. Antennas Propagat.*, vol. 58, no. 1, pp. 227-229, Jan. 2010.

[9] Q. H. Liu, "The PSTD algorithm: A time-domain method requiring only two cells per wavelength," *Microw. Opt. Tech. Lett.*, vol. 15, no. 3, June 20, 1997.

[10] Q. L. Li and Y. C. Chen, "Application of the PSTD for scattering analysis," *IEEE Trans. Antennas Propag.*, vol. 50, no. 9, pp. 1317-1319, Sep. 2002.

[11] J. P. Berenger, "A perfectly matched layer for the absorption of electromagnetic waves," *J. Computat. Phys.*, vol. 114, pp. 185-200, 1994.

[12] J. Chen and J. G. Wang, "Weakly conditionally stable and unconditionally stable FDTD schemes for 3D Maxwell's equations," *Progr. Electromagn. Res. B*, vol. 19, pp. 329-366, 2010.

[13] J. Chen and J. G. Wang, "A novel hybrid implicit explicit – pseudospectral time domain method for TMz waves," *IEEE Trans. Antennas Propag.*, vol. 61, no. 7, July 2013.

[14] J. Chen and J. G. Wang, "A three-dimensional HIE-PSTD scheme for simulation of thin slots," *IEEE Trans. Electromagn. Compat.*, vol. 55, no. 6, Dec. 2013.

[15] J. Chen and J. G. Wang, "A WCS-PSTD method for solving electromagnetic problems both with fine and electrically large structures," *IEEE Trans. Antennas Propag.*, vol. 62, no. 5, May 2014.

[16] W. K. Leung and Y. Chen, "Transformed-space non-uniform PSTD algorithm," *Microwave Opt. Technol. Lett.*, vol. 28, 2003.

Jianying Guo received the B.S. degree in Electronic Technique from Henan Normal University, Xin'xiang, China, in 1996, and is currently working toward the Ph.D. degree in Electromagnetic Fields and Microwave Techniques at Xi'an Jiaotong University, Xi'an, China.

Her current research interests include computational electromagnetics, especially the FDTD method, microwave devices design and terahertz electronics.

Juan Chen was born in Chongqing, China, in 1981. She received the Ph.D. degree in Electromagnetic Field and Microwave Techniques from the Xi'an Jiaotong University, Xi'an, China, in 2008.

She is currently an Associate Professor at Xi'an Jiaotong University. Her research interests include numerical electromagnetic methods, antenna designs, and electromagnetic compatibility.